JOURNAL OF AGRICULTURAL AND FOOD CHEMISTRY

ARTICLE

pubs.acs.org/JAFC

Monitoring Protein Structural Changes and Hydration in Bovine Meat Tissue Due to Salt Substitutes by Fourier Transform Infrared (FTIR) Microspectroscopy

Nebojsa Perisic,*[,†,§] Nils Kristian Afseth,[†] Ragni Ofstad,[†] and Achim Kohler[†,#]

[†]Nofima AS, Osloveien 1, 1430 Ås, Norway

[§]Institute of Mathematical Sciences and Technology, Norwegian University of Life Sciences, P.O. Box 5003, 1432 Ås, Norway

[#]Centre for Integrative Genetics (CIGENE), Department of Mathematical Sciences and Technology (IMT), Norwegian University of Life Sciences, 1432 Ås, Norway

ABSTRACT: The objective of this study was to investigate the influence of NaCl and two salt substitutes, $MgSO_4$ and KCl, in different concentrations (1.5, 6.0, and 9.0%) on meat proteins by using Fourier transform infrared (FTIR) microspectroscopy. Hydration properties and secondary structural properties of proteins were investigated by studying the amide I, amide II, and water regions (3500−3000 cm^{-1}) in FTIR spectra. By applying multivariate analysis (PCA and PLSR), differences between samples according to salt concentration and salt type were found and correlated to spectral bands. The most distinctive differences related to salt type were obtained by using the water region. It was found that samples salted with $MgSO_4$ exhibited hydration and subsequent denaturation of proteins at lower concentrations than those salted with NaCl. Samples salted with KCl brines showed less denaturation even at the 9.0% concentration. The FTIR results were further supported by water-binding capacity (WBC) measurements.

KEYWORDS: FTIR microspectroscopy, protein secondary structure, hydration, myofibrillar proteins, salt substitutes, WBC

INTRODUCTION

In recent years, the increased consumption of dietary sodium seen in the Western world has been linked to detrimental health effects.[1−3] Thus, a need for reducing NaCl in highly consumed food products such as processed industry foods[4,5] has emerged. Apart from lowering the level of added salt (NaCl) in processed foods, there are several major approaches in reducing the sodium level, with utilization of salt substitutes being the most frequently used alternative.[4−6] However, NaCl displays multiple functional roles in processed foods: it increases water-binding capacity (WBC), inhibits microbial growth, and improves taste and processability.[5] In muscle foods, many of these properties are connected to the meat protein structure, particularly texture, tenderness, and WBC.[5,7] When NaCl is reduced or replaced, these properties inevitably change.

During the past decade a number of salt replacers have become commercially available.[8] An appropriate salt replacer needs to have acceptable sensory properties as well as functional properties. Two candidates for successful salt replacers are KCl and $MgSO_4$, with KCl being one of the most common NaCl substitutes nowadays.[6,9,10] $MgSO_4$, on the other hand, is used in some commercially available salt mixtures, replacing pure NaCl.[5,11]

The interaction of NaCl with the food matrix has been studied by many authors,[4,9,10,12−15] but the biophysical rationale behind the mechanisms of the interaction between NaCl and the protein matrix in muscle foods is still only partially understood. In recent years, Fourier transform infrared (FTIR) microspectroscopy has been used for monitoring conformational changes of myofibrillar proteins. By utilization of FTIR microspectroscopy, in situ spectra of single myofibrillar cells can be obtained. Böcker et al. showed by employing FTIR microspectroscopy that changes in tertiary structure of the myofibers during swelling and shrinkage may be directly related to changes in the secondary structure of myosin molecules.[16] FTIR microspectroscopy has also been employed to study conformational changes in proteins as a function of salt concentration.[16] Furthermore, in combined FTIR and low-field NMR studies conformational changes in proteins due to different salt concentrations have been related to water-binding properties.[17,18] Because it is very likely that salt replacers change the biophysical situation on a molecular level, similar studies involving different salt replacers are urgently needed. Moreover, it is known that FTIR spectroscopy can also provide information about water molecules interacting with protein molecules and salt ions.[19−21] This potential has yet to be utilized for studying the interaction between salt substitutes and meat matrices.

The main objective of this study was to investigate and assess the differences in the effects of NaCl, KCl, and $MgSO_4$ on the protein structure and hydration properties in bovine meat using FTIR microspectroscopy. To do this we used FTIR spectra to (I) determine changes in protein secondary structure and water interactions through analyzing the amide I (1600−1700 cm^{-1}) and amide II regions (1500−1600 cm^{-1}); (II) assess and estimate the interaction of protein molecules with water through analyzing the region between 3000 and 3500 cm^{-1}, denoted as the "water region" that also includes amide A and amide B

Received: April 19, 2011
Revised: August 10, 2011
Accepted: August 10, 2011
Published: August 10, 2011

bands,[22] as well as information about the OH stretching vibration of water molecules; and (III) correlate these different sample characteristics by using multivariate analytical methods based on latent variables, such as principal component analysis (PCA) and partial least-squares regression (PLSR).

Band assignment of respective underlying bands in all selected regions has also been attempted in accordance with both the literature and multivariate data analysis. In addition, measurement of the WBC of brined meat was performed to validate the results obtained by FTIR microspectroscopy.

MATERIALS AND METHODS

Sample Preparation. Samples of beef muscle (longissimus dorsi) were obtained from four different animals (Norwegian Red breed) at 48 h post rigor (obtained from a commercial slaughter). From each animal, two muscle blocks of approximately 4 × 4 × 1 cm were excised and placed in each of nine different salt brines. The salt brines were composed of pure NaCl, KCl, and $MgSO_4$ (Merck, Darmstadt, Germany) solutions, made in 1.5, 6.0, and 9.0% total salt weight percentage concentrations. To avoid dilution of the salt brines, the mass ratio of meat to brine was set to approximately 1:8. The samples were kept in brines at 4 °C for 48 h with 0.05% NaN_3 added to prevent any possible deterioration caused by microbial growth.

Water-Binding Capacity. Commercially available fresh samples of beef muscle (longissimus dorsi) were obtained and consecutively brined in the same way as aforementioned. From each of the four commercial packages two slices of 3 × 3 × 1 cm were excised and placed in each brine, resulting in a total of eight replicates in each of the nine salt brines. Afterward, the expressed juice was measured by using the filter paper press method:[23] meat samples were placed between five layers of filter paper (Whatman no. 1, 70 mm diameter) and consecutively pressed by aluminum plates using a TA.HDi Texture Analyzer (Stable Micro Systems Ltd., Godalming, U.K.), with a velocity of 0.8 mm/s, until a 50% reduction of the sample thickness. After the 50% sample thickness reduction was reached, the plates were immediately pulled back. The percentage of expressed juice was calculated as the mass of expressed juice divided by the initial sample mass (i.e., the sample mass before applying pressure).

FTIR Microspectroscopy. For FTIR microspectroscopic measurements, two muscle blocks of approximately 1.0 × 0.6 × 0.3 cm were excised from each of the muscle samples, consecutively embedded in OCT compound (Tissue-Trek, Electron Microscopy Sciences, Hatfield, PA), and snap-frozen in liquid N_2. Afterward, all of the samples were transferred to a −80 °C freezer, where they were stored until cryo-sectioning, which was performed transversely to the fiber direction on a Leica CM 3050 S cryostat (Leica Microsystems Wetzlar GmbH, Wetzlar, Germany). The sections were cut in 10 μm thickness, thaw-mounted on infrared transparent ZnSe slides, and subsequently stored in a desiccator before acquisition of the FTIR spectra.

Acquisition of FTIR spectra was performed on an IRScopeII FTIR microscope coupled to an Equinox 55 FTIR spectrometer (Bruker Optik GmbH, Ettlingen, Germany), equipped with a liquid nitrogen-cooled mercury cadmium telluride (MCT) detector. Spectra were collected from single myofibers in transmission mode in the range from 4000 to 1000 cm^{-1}, with spectral resolution of 4 cm^{-1} using a 15× objective lens.

For each spectrum 64 interferograms were collected and averaged. Both spectrometer and microscope were sealed by a specially designed box and were continuously purged with dry air to reduce the spectral contribution of water vapor and CO_2. Additional compensation for water vapor/CO_2 variation was accomplished by taking background spectra of the ZnSe substrate. From each of the snap-frozen meat blocks (1.0 × 0.6 × 0.3 cm) two cryosections were excised, and from each of the cryosections 15 spectra were obtained on different single myofibers. This resulted in the acquisition of 30 spectra per experimental treatment and animal. The final data set consists of 1080 spectra (30 spectra times 4 animals times 9 brines).

Data Analysis. Spectra were subjected to a quality test developed by Bruker (Bruker Optik GmbH), which involves testing spectra for signal-to-noise ratio, signal intensity, and water vapor amount within the predefined limits for each of the criteria. Spectra not passing the predefined limits were removed.

Second derivatives of the spectra were calculated using the Savitzky−Golay algorithm[24] to resolve the overlapping bands of individual vibrations in three different regions: water region (3500−3000 cm^{-1}), amide I region (1700−1600 cm^{-1}), and amide II region (1600−1500 cm^{-1}). Because the bands in the water region are generally much broader and the water region is also subjected to a higher level of water vapor, a bigger window for calculating second derivatives by the Savitzky−Golay algorithm was used in this region: a window of 37 smoothing points was used for the water region, whereas in the amide I and amide II regions, we applied a window size of 11 smoothing points. Because spectral reading was approximately one absorbance value per cm^{-1}, the window size for calculating second derivatives in the water region corresponds to approximately 36 cm^{-1}, whereas in the amide I and II regions it corresponds to approximately 11 cm^{-1}.

The spectra were thereafter averaged by taking the mean of all replicate spectra of the same muscle block, resulting in four spectra per brine and animal (2 muscle blocks times 2 cryosections). Afterward, the spectra were preprocessed using extended multiplicative signal correction (EMSC)[25,26] at 1800−1000 cm^{-1} for the amide I and II regions and at 4000−1000 cm^{-1} for the water region bands. This provides the ability to separate and characterize the unwanted physical effects (e.g., differences in sample thickness and light scattering) and desired chemical information (e.g., protein secondary structure) that are contained in the spectra.[25]

After preprocessing, the data were analyzed by principal component analysis (PCA) and partial least-squares regression (PLSR).[27] PCA was used to study the unsupervised variation pattern in the data,[28] and PLSR was performed to relate different spectral regions. In PLSR models, the water region was used as the *X* matrix, whereas as the *Y* matrix amide I and amide II regions were used separately. Correlations between FTIR variables, design variables, and latent variables were studied by correlation loading plots, in which the correlations between variables and PLS/PCA score vectors are plotted. In correlation loading plots both variables that were part of the PCA/PLSR modeling and variables that were kept outside the modeling step were plotted. Design variables were never used to build PCA or PLSR models. When design variables were plotted in correlation loading plots, they were defined as indicator variables, that is, one column for each design variable in which 1's and 0's indicate if the sample belongs to the respective design condition or not, respectively. All PCA and PLSR results are consecutively validated by cross-validation,[29,30] where samples referring to the same animal are taken out in each cross-validation loop. All variables are divided by their standard deviation before analysis by PCA and PLSR.

For calculating PCA and PLSR models, whole FTIR regions including all variables were used. For the sake of clarity, the correlation loading plots were presented by using only positions of the minima in second-derivative spectra, which correspond to positions of band maxima in nonderivative spectra. Certain FTIR bands exhibit shifts in minimum positions. In the plots this is manifested as continual assembly of variables close to each other and is particularly visible in water region variables.

Preprocessing and data analysis were performed using in-house developed routines written in MATLAB (version 7.10, The MathWorks, Natick, MA) and The Unscrambler (version 10.1, CAMO Process AS, Oslo, Norway).

RESULTS

Band Assignment. Examples of FTIR spectra obtained from single myofibers from tissue sections are shown in Figure 1.

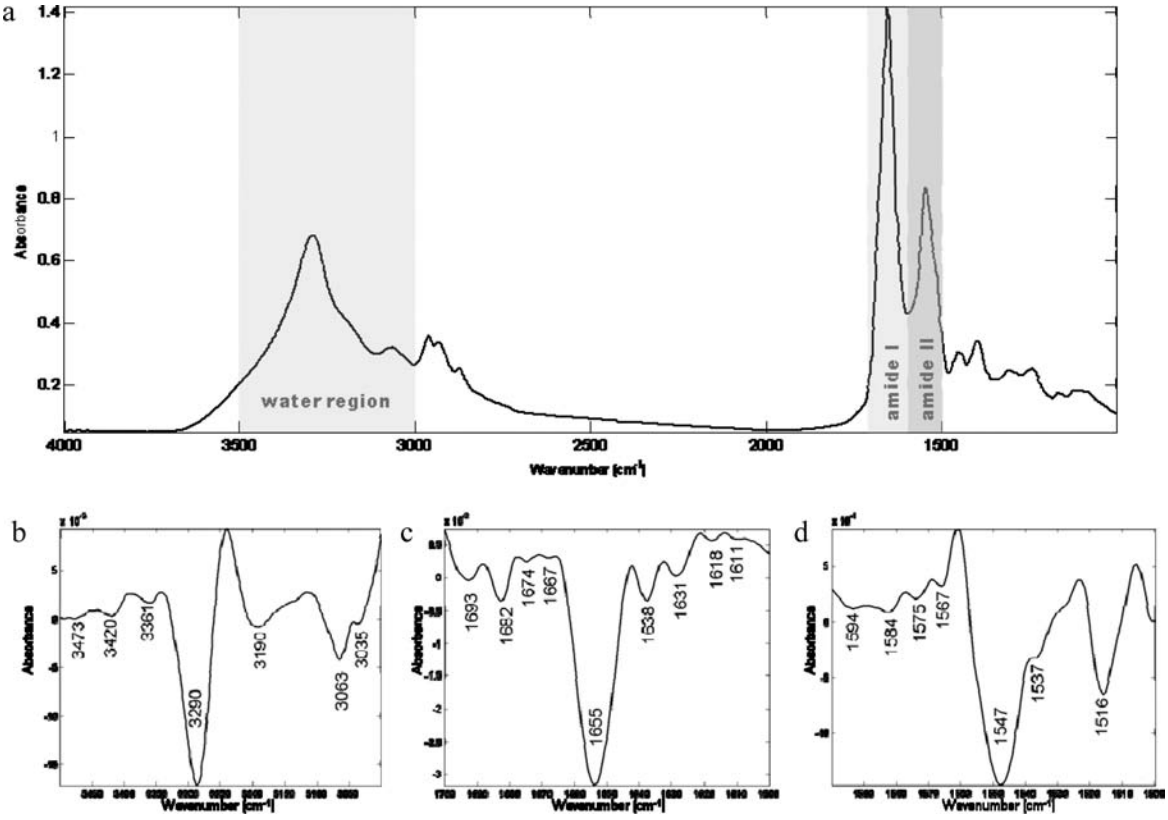

Figure 1. (a) Typical FTIR spectrum presented in the whole spectral region from 4000 to 1000 cm^{-1}. Second derivatives of each of the selected regions are shown for the water region (b), the amide I region (c), and the amide II region (d).

Specific regions of the FTIR spectra that were used for the analysis are marked with gray shading in Figure 1a and include the water region (3500−3000 cm^{-1}), the amide I region (1700−1600 cm^{-1}), and the amide II region (1600−1500 cm^{-1}). Second-derivative spectra of these three regions are shown in Figure 1, panels b, c, and d, respectively. Correspondingly, a summary of tentative assignments of the bands, which is in accordance with our previous work and the literature,[18,31] is given in Table 1. As has been shown, each of these regions provides a specific type of information on protein structure and protein hydration, which is available through analysis of the properties of vibrations that the specific region is composed of. More specifically, the amide I region (1700−1600 cm^{-1}) presented in Figure 1c provides detailed information about the protein backbone, mainly through dominating contributions of the C═O stretching vibration.[20,32] Due to its high sensitivity to protein secondary structure, the amide I band is often used to study protein folding, unfolding, and aggregation. The amide II region (1600−1500 cm^{-1}) that is presented in Figure 1d consists mainly of N—H in-plane bending and C—N stretching vibrations.[32] The assignment of bands in the amide II region is not as clear as in the amide I region, which is why the latter region is often preferred in protein structure analysis by FTIR spectroscopy.[22] Finally, the water region (3500−3000 cm^{-1}) presented in Figure 1b consists mostly of N—H stretching vibrations and O—H stretching bands, including the amide A and B bands.[19,22]

PCA Results: Protein−Water Interactions. To study differences in protein structures and hydration properties as a function of salt concentration and salt type, PCA was performed on second-derivative spectra of the amide I region and the water region, separately. Score plots for the first and second principal components (PCs) for both regions are presented in Figure 2. Score plots of the amide I region variables are presented in the top row of Figure 2 (panels a and b), whereas score plots of the water region variables are presented in the second row (panels c and d). Labeling of samples was done with respect to the experimental design: salt concentration label (left column of Figure 2, panels a and c) and salt type label (right column of Figure 2, panels b and d).

Amide I. As can be seen in Figure 2a, the effect of salt concentration spans most of the variation in the amide I variables, causing samples that are treated with different salt concentrations to cluster together. The calibrated explained variance for PC1 is 54.5%, whereas the validated explained variance is 53.6%. The first PC accounts for most of this concentration effect, because the major part of the 9% samples is clearly separated from the rest of the samples along PC1. Furthermore, in the same figure it is visible that the 1.5% samples are clearly separated from the rest of samples along PC2. The calibrated explained variance for PC2 is 16.9%, whereas the validated explained variance is 16.5%. It can be seen that within the different concentration clusters (visible in Figure 2a), there is a minor degree of separation with respect to salt type (Figure 2b). The effect of different animals was also investigated, but the score plots did not show any visible clustering of samples due to animal type (results not shown). This leads to the conclusion that the effect of different animals is much smaller than the effects of salt type and salt concentration and that this effect as such does not significantly affect the differentiation between samples.

Water Region. Unlike in the amide I region, clustering of samples is visible for both salt type and salt concentration in the water region as presented in Figure 2c,d. Within the clusters due

Table 1. Band Positions and Assignments for the Amide I, Amide II, and Water Regions According to the Literature and Our Previous Work

region	freq (cm^{-1})	tentative assignment[a]
amide I	1693	aggregated β-sheet structures (sideband of 1631 cm^{-1} band),[32−35] M/P
1700−1600 cm^{-1}	1682	native (parallel/antiparallel) β-sheet structures,[20,32,33,37] M/P/T
(80% C═O stretch,	1674	tentatively assigned to turns,[22] M/P
10% C—N stretch,	1667	nonhydrogenated C═O group, internal random coil segments that are not involved in H-bonding,[33,35] M/P
10% N—H bend)	1660	loop structures/α-helical structures,[16,43,51] M/P
	1655	α-helical structures, C═O stretching vibrations originating from α-helical structures in the myofibrillar proteins,[20,32,33,37] M/P/T or water vibration [36,38] P
	1638	water deformation mode in liquid water [19,52] P or native (parallel/antiparallel) β-sheet structures,[22,33] M/P/T
	1631	aggregated β-sheet structures,[32−35] M/P
	1618	aggregated β-sheet structures,[16,43,51] M
	1611	tyrosine amino acid side chain vibrations[33,40] or aggregated strands,[41] M/P
amide II	1594	not assigned
1600−1500 cm^{-1}	1584	α-helical structures,[33] M
(60% N—H bend,	1575	amide II unspecified,[33] M
40% C—N stretch)	1567	residue and/or possibly aggregated β-sheet structures,[33,42] M
	1547	α-helical structures,[33] M/P
	1537	possibly aggregated β-sheet structures,[33] M
	1516	possibly tyrosine,[33] M/P
water region	3473	nonhydrogenated N—H groups,[19,22,39] P
3500−3000 cm^{-1}	3420	hydrogenated N—H groups or O—H stretching band,[21,22,39,53] T/P
(N—H stretching,	3361	companion band of 1530 cm^{-1} band, in solution occurring at 3345 cm^{-1}, and/or N—H stretching band,[21,39] T/P
C—N—H stretching vibration,	3290	N—H stretching band/amide A,[21,22,39,42] T/P, or hydrogen-bonded NH groups [19] P
O—H stretching vibration)	3190	not assigned
	3063	N—H stretch/amide B/amide II overtone/amide II combination mode in β-sheet structures,[22,39] T/P
	3035	not assigned

[a] M, obtained in real meat system; P, obtained in pure protein or polypeptide model system; T, obtained by theoretical calculation and/or prediction.

to salt type, subclusters due to concentration are also visible. The calibrated explained variance for PC1 is 60.5%, whereas the validated explained variance is 60.3%. In the first PC a clear distinction between KCl and NaCl brines is visible, whereas the difference between $MgSO_4$ (bottom) and NaCl and KCl brines (top) is visible in PC2. The calibrated explained variance for PC2 is 18.1%, whereas the validated explained variance is 17.9%. Similarly to the amide I region, clusters due to the different animals are not visible in score plots of water region variables (results not shown).

To assess specific spectral features that cause the distinction of the samples presented in the PCA score plots, the corresponding correlation loading plots are displayed. The correlation loading plots of these PCA models are presented in Figure 3. More precisely, Figure 3a depicts the correlation loading plot of PC1 and PC2 of the amide I region, including design variables. Equivalently, Figure 3b depicts the correlation loading plot of PC1 and PC2 of the water region variables, including design variables. Because the score plots showed tendencies of interactions between certain salt types and concentrations such as between $MgSO_4$ salt type and 6% concentration, all possible interactions between design variables are included and presented in the plots. Interaction variables are simply calculated as products of the design variables.

Amide I (See Figure 3a). The main variation in the *positive* direction of PC1 is due to variables around bands assigned to aggregated β-structures at 1630 and 1693 cm^{-1} [32−35] and antiparallel β-structures at 1683 cm^{-1}.[22,33] In some specific cases these bands are also associated with protein hydration differences.[19] The main variation in the *negative* direction of PC1 is due to variables around a band at 1655 cm^{-1} related to native α-helical structures and water vibration[20,32,33,36−38] and variables around a yet nonassigned band at 1614 cm^{-1}. Thus, the design variables 9% salt concentration, 9% NaCl, and 9% $MgSO_4$ brines are strongly *positively* correlated to bands attributed to aggregated β-structures. The main variation in PC2 may be explained by a shift of the band at 1655 cm^{-1} from higher to lower wavenumbers, whereas the lower wavenumbers are shifted toward the *positive* direction of PC2. In addition to this, a band assigned to nonhydrogenated C═O groups at around 1668 cm^{-1} [32,35] and a band tentatively assigned to turns[22] at 1674 cm^{-1} are *negatively* correlated to PC2. The design factors related to 1.5% salt concentration brines and 1.5% NaCl brines are both *positively* correlated to PC2, although this correlation is not very strong.

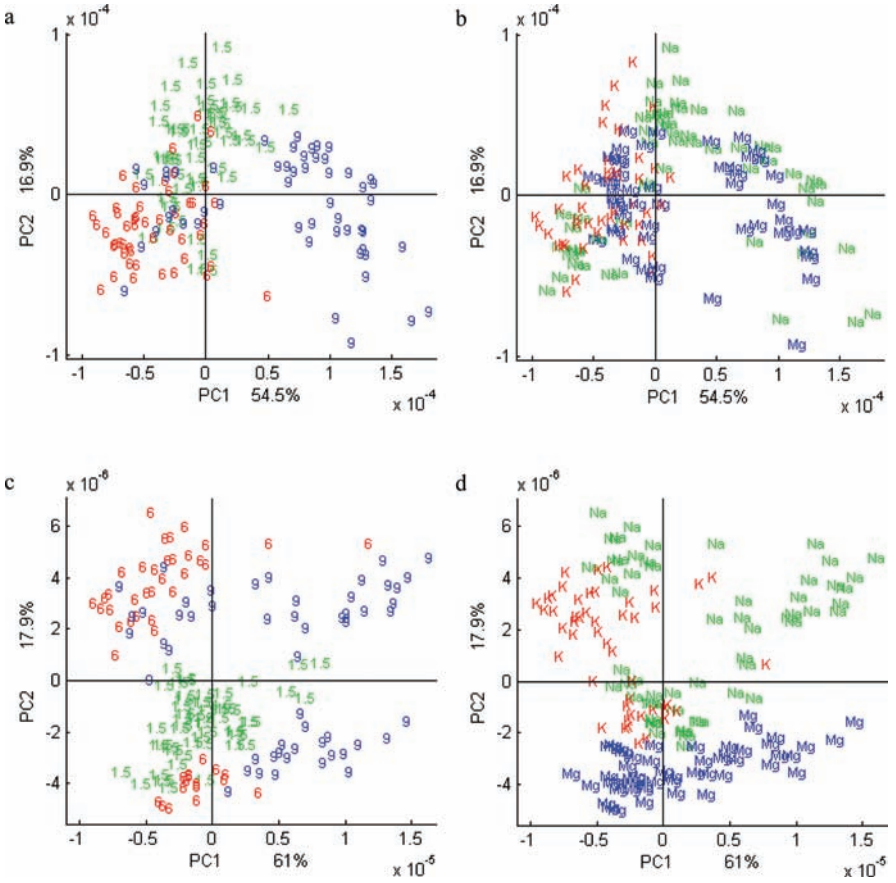

Figure 2. PCA score plots for the first and second PCs are shown for the amide I region (a, b) and the water region (c, d). In the left column (a, c), samples are labeled according to salt concentration, whereas in the right column (b, d), samples are labeled according to salt type.

Water Region (See Figure 3b). The first PC of the PCA model of the water region variables is explained by a shift from wavenumber 3283 cm^{-1} to wavenumber 3290 cm^{-1}. The corresponding band around 3290 cm^{-1} is assigned to the amide A band (between 3270 and 3310 cm^{-1}), which is exclusively located on the NH group and for that reason is not sensitive to the conformation of the polypeptide backbone in proteins.[22] However, the frequency of this band depends on the strength of the hydrogen bond.[22] A band around 3063 cm^{-1} and a band around 3361 cm^{-1} explain a major part of the variation along PC2. The band around 3063 cm^{-1} together with the design factors related to NaCl salt brines is *positively* correlated to PC2. This band is assigned to amide B, the second part of the Fermi resonance doublet (with amide A being the first part) absorbing weakly between 3100 and 3030 cm^{-1}.[22] In small peptide molecules this band is attributed to the overtone of the amide II vibration, and in β-sheet structures it is associated with the amide II combination mode.[22] Alternatively, this same band is assigned to NH stretching vibrations of intramolecularly hydrogen-bonded NH groups.[22,39] The band at 3361 cm^{-1}, which is *negatively* correlated with PC2, is assigned to both the N−H stretching band and the amide II overtone.[19,22,39] A band around 3420 cm^{-1},[19,22] which is assigned to nonhydrogenated NH groups, and a band around 3120 cm^{-1}, which is not assigned (and also appears as a shoulder to the 3190 cm^{-1} band), are also *negatively* correlated to PC2. Design variables related to KCl brines are weakly *negatively* correlated to PC1. The design variables referring to $MgSO_4$ brines are *negatively* correlated to PC2 and, therefore, strongly *positively* correlated to nonhydrogenated NH groups.

In addition to this, higher principal components were also taken into consideration (data not shown). The variation explained by these components enabled only the distinction between low (1.5%) and higher (6 and 9%) salt concentrations (only in PC3 and PC4), and no significant variance due to different salt types was found.

PLSR Results. To relate information about protein conformations, hydrogen bindings, and water, a PLSR was performed. For this purpose water region variables were used as *X*, and the amide I and II regions were defined as *Y*. The corresponding correlation loading plots are shown in Figure 4, panels a and b, respectively. Design variables including interactions between salt concentrations and salt types were pacified in the calculation of the PLSR models, such that they did not affect the model. The *X* variables are plotted in black color, *Y* variables in blue, and design variables in green. It can be seen that all applied salt types explain variations with respect to secondary structure of proteins combined with protein hydration (both amide I and amide II defined as *Y* variables) and their hydration properties (*X* variables). The same is apparent for the applied concentrations.

Amide I (Y) and Water Region (X) (Figure 4a). The first component explains 30.4/27.6% of the variance in the *X* and *Y* blocks, respectively. After validation of this model by cross-validation, the explained variance for PC1 is 29.3/26.6% for *X* and *Y*, respectively. Furthermore, bands at 1631 cm^{-1} (aggregated β-structures),[32−35] 1682 cm^{-1} (antiparallel β-sheet

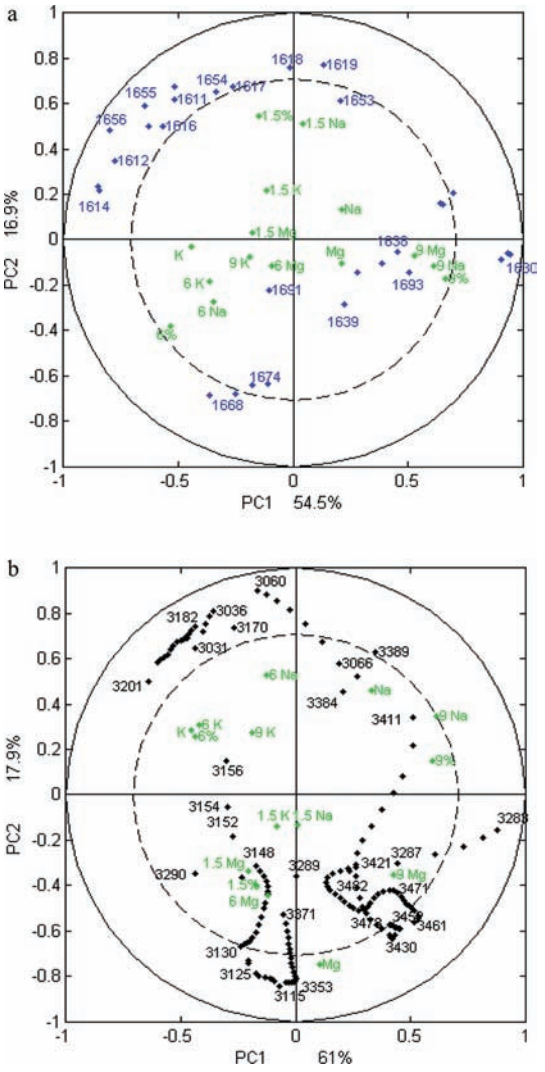

Figure 3. Correlation loading plots of the first and second components for PCA models of the amide I region (a) and the water region (b). Pacified design variables are plotted in green color including interactions between different salt concentrations and different salt types.

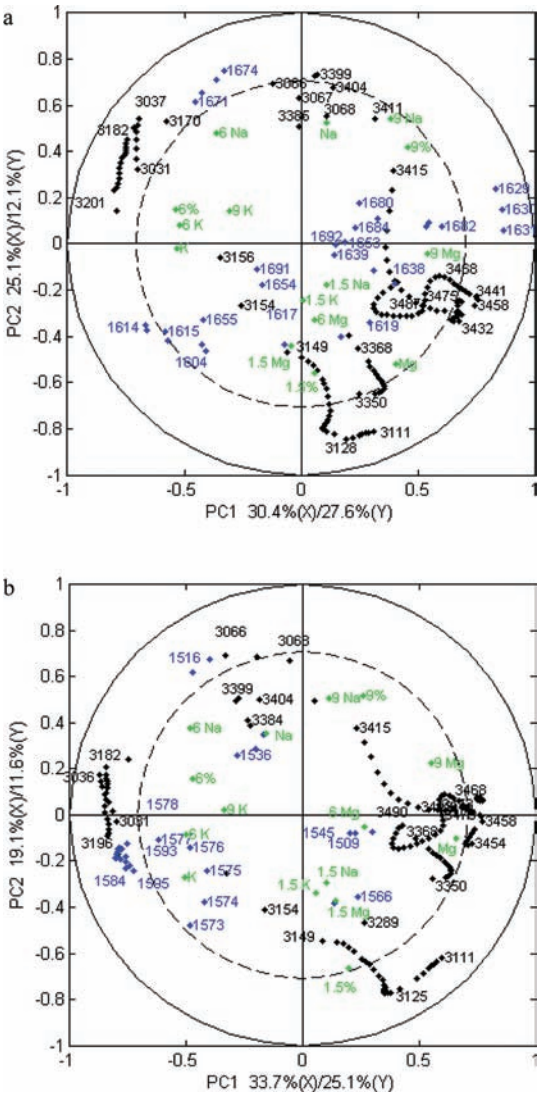

Figure 4. Correlation loading plots of the first and second components for PLSR models using the water region as *X* and amide I region as *Y* (a); (b) corresponding correlation loading plot using the amide II region as *Y*. Water region variables are plotted in black color, amide I variables in blue, and pacified design variables in green.

structures),[20,32,33,37] 1638 cm^{-1} (assigned to aggregated β-structures or water deformation mode),[36,38] and around 3400 cm^{-1} (assigned to hydrogenated N−H groups or OH stretching vibration)[19,22,39] are *positively* correlated to PC1 and therefore also *positively* correlated to design variables 9% $MgSO_4$, $MgSO_4$, and 9% concentration. The main variation in the *negative* direction of PC1 is due to bands at 1655 cm^{-1} (α-helical structures), 1616 cm^{-1} (possibly tyrosine),[33,40] 1674 cm^{-1} (turns), and 3190 and 3035 cm^{-1} (not assigned). The band at around 1655 cm^{-1} is also known to be related to water vibrations.[36,38] However, in our correlation loading plots this band is always negatively correlated to vibrational bands of hydrogenated NH groups and water bending vibration (located at above 3400 cm^{-1} and 1638 cm^{-1}, respectively) and therefore we are mainly attributing it to protein α-helical structures and corresponding hydration changes. The design variables 6% salts, 6% KCl, KCl brines, and 6% NaCl brines are also *negatively* correlated to PC1. The second component explains 25.1/12.1% of the variance in the *X* and *Y* blocks, respectively (after cross-validation, 24.9/11.6%). In the *positive* direction of PC2 the main variation is due to N−H stretching vibration at 3063 cm^{-1} (somewhat ambiguously assigned to amide II overtone, amide B, and intramolecularly hydrogen-bonded NH groups)[22,39] and 1674 cm^{-1}. The design variable 6% NaCl is close to the band at 1674 cm^{-1} in the correlation loading plot. Design variables 9% NaCl, 6% NaCl, and NaCl are *positively* correlated to PC2 and thus to amide II overtones. Variables around 3125 cm^{-1} and a band at 1618 cm^{-1} contribute the most to the main variation in the *negative* direction of PC2. The variables around 3125 cm^{-1} refer to an unassigned and very weak shoulder in the spectra, whereas the band around 1618 cm^{-1} has previously been assigned to tyrosine[40,41] or protein−water interaction in casein micelle investigation.[36] Both bands are strongly *positively* correlated to the design variables 1.5% $MgSO_4$, 6% $MgSO_4$, and $MgSO_4$ as well as to design variables 1.5% KCl and 1.5%.

Amide II (Y) and Water Region (X) (Figure 4b). The first component explains 33.7/25.1% of the variation in the *X* and *Y*

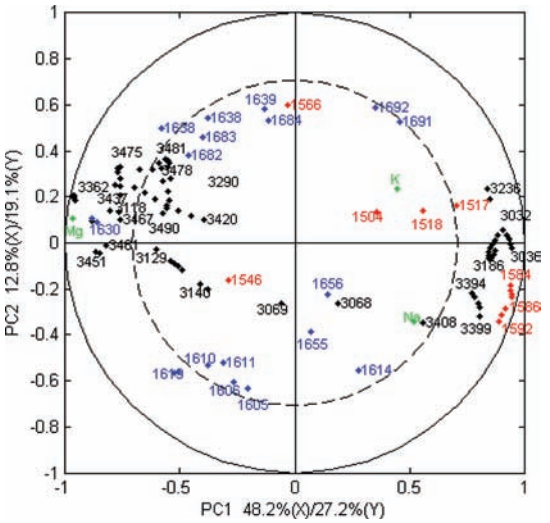

Figure 5. Correlation loading plot of the first and second components for PLSR model using the water region as *X* and amide I region as *Y*. This PLSR model is calculated for 6% concentrations only. Water region variables are plotted in black color, amide I variables in blue, and pacified amide II and design variables in red and green, respectively.

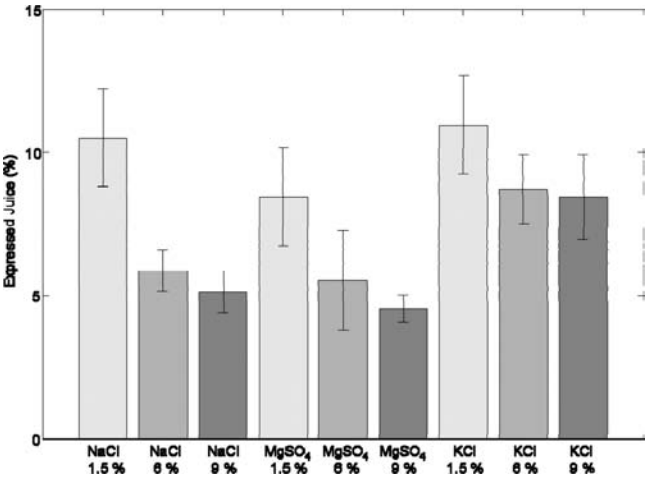

Figure 6. Water-binding capacity of samples treated with different salt brines plotted with 2-fold standard deviation of the mean value (corresponding to a 95% confidence interval):[54] light gray bars represent the 1.5% concentration, medium gray bars the 6% concentration, and dark gray bars the 9% concentration; the first three bars depict NaCl brines, the second three, $MgSO_4$ brines, and last three, KCl brines.

blocks, respectively (after cross-validation, 32.8/24.3%). The variation in the *positive* direction of PC1 is mostly due to bands assigned to nonhydrogenated N−H groups above 3400 cm^{-1}. These bands are strongly correlated to $MgSO_4$ brines, because the design variables 6% $MgSO_4$, 9% $MgSO_4$, and $MgSO_4$ are all *positively* correlated to PC1, whereas 9% $MgSO_4$ and $MgSO_4$ are somewhat more strongly correlated. The main variation in the *negative* PC1 direction is mainly due to a band at 1584 cm^{-1} assigned to α-helical structures[33] and bands at 3190 and 3035 cm^{-1} (both not assigned) and a band around 1575 cm^{-1}, which is assigned to amide II without further specification.[33] These bands are *positively* correlated to the design variables KCl brines, 6% KCl, and 6% concentration. PC2 accounts for 19.1/11.6% of the variance in the *X* and *Y* blocks, respectively (after cross-validation, 17.34/9.3%). The main variation in the *positive* direction of PC2 is due to the band at 1516 cm^{-1}, which is assigned to tyrosine,[33,40] and a band at 3063 cm^{-1} assigned to the N−H stretching band of the amide II overtone.[22,39] The design variables 9% brines, 6% NaCl, and 9% NaCl are *positively* correlated to these bands. The main variation in the *negative* PC2 direction is due to variables close to but below the band at 1572 cm^{-1} (not assigned) with a very weak contribution of the band at 1567 cm^{-1}, which is ambiguously assigned to either amino acid side-chain residues[22,42] or aggregated β-structures.[33] Design variables that are closely related to these bands are 1.5% brines and 1.5% NaCl, 1.5% KCl, and 1.5% $MgSO_4$ brines.

PLSR models were also established by splitting the data in subsets, where each subset corresponded to one concentration (1.5, 6, and 9% brines). For each concentration separately, the variation introduced by the different salt types was studied. In Figure 5, the correlation loading plot for the PLSR model of the 6% concentration is presented. The model was calculated using water region variables as *X* variables and amide I variables as *Y* variables, whereas amide II and design variables were pacified and plotted together with the other variables in the correlation loading plot. The first component explains 48.2/27.2% of the variation in the *X* and *Y* blocks, respectively (after cross-validation, 45.4/23.3%). The main variation in the *positive* direction of PC1 is caused by variables around the bands at 1674 cm^{-1} (turns), 3035 cm^{-1} (not assigned), and 3190 cm^{-1} (not assigned). All of these bands are strongly *positively* correlated to variables around the amide II bands at 1594 and 1584 cm^{-1}. The main variation in the *negative* direction of PC1 is caused by the variables around the bands at above 3400 cm^{-1} (hydrogenated N−H groups), at 3290 cm^{-1} (N−H stretching band, amide A, or hydrogen-bonded NH groups),[21,22,39,42] at 1631 cm^{-1} (aggregated β-structures), and at 1682 cm^{-1} (antiparallel β-structures). All of these bands are strongly *positively* correlated to $MgSO_4$ salts. The second component explains 12.8/19.1% of the variation in the *X* and *Y* blocks, respectively (after cross-validation, 5.2/3.6%). Variables around the amide I bands at 1638, 1690, and 1682 cm^{-1} are *positively* correlated to PC2 and thus *positively* related to bands around the 1537 cm^{-1} band, which have been assigned to aggregated β-structures. Variables around the bands at 1611 and 1618 cm^{-1} are *negatively* correlated to PC2.

Water-Binding Capacity (WBC). To elucidate the relationship between WBC and the observed differences in protein hydration and denaturation characteristics between the different salts, an additional experiment was performed. The results from WBC measurements are presented in Figure 6, where the percentage of expressed juice is plotted for each brine. As can be seen, the overall trend is that with increasing concentration of salt, the amount of expressed juice decreases (from 10.5 to 5.1% for NaCl brines, from 8.4 to 4.5% for $MgSO_4$, and from 11.0 to 8.4% for KCl brines), which directly corresponds to increased WBC. The highest WBC (lowest amount of expressed juice) in the 1.5% concentration range is found in samples treated with $MgSO_4$ (8.4%), whereas the lowest WBC is found for KCl (11.0%), which was also close to samples treated with NaCl (10.5%). Overall, samples treated with $MgSO_4$ exhibit higher similarity to samples treated with NaCl than to samples treated with KCl. Finally, samples treated with $MgSO_4$ brines exhibit the highest WBC in all of the applied concentrations. The results obtained by WBC measurements show a high correspondence to the results obtained by FTIR microscopy. This again shows that

the changes in the secondary structure of the myofibrillar proteins can be connected to macroscopic properties of meat, such as WBC.

DISCUSSION

Myofibrillar Proteins: Secondary Structure, Hydration, and Denaturation. Salting of meat is associated with changes in the water-binding capacity of the meat proteins, and it is also linked to protein destabilization and denaturation when salt concentration increases.[16,33] Destabilization and denaturation of proteins in meat tissues as well as their hydration can be monitored in the amide I region (1700−1600 cm^{-1}) and the water region (3500−3000 cm^{-1}) of FTIR spectra. The amide I region (Figure 1b) provides detailed information about protein backbone, mainly through dominating contributions of the C═O stretching vibration.[20,32] Analysis of the PCA score plots made on the amide I region (Figure 2a−c) reveals that the main variation pattern in the amide I region is caused by differences in salt concentration. This difference in salt concentration also seems to be the main factor for protein secondary structural changes in the meat proteins in the present experiment. When examining the corresponding correlation loading plot in Figure 3a, we can see that high salt concentrations are related to the band at ∼1631 cm^{-1} together with a weaker band at around 1693 cm^{-1}, which have been assigned to aggregated β-structures in meat tissue samples.[32,34,35] The increase in intensity of this band corresponds to increases in amounts of aggregated β-structures. This is also often followed by a decrease in intensity of the band at ∼1655 cm^{-1}, a pronounced intense band with a weak shoulder occurring at lower wavenumbers that can be assigned to C═O stretching vibrations originating from α-helical structures in the myofibrillar proteins[20,32,33,37] and to water vibrations.[36,38] Conversely, the α-helical band around 1655 cm^{-1} is located at the opposite side of the aggregated structures and hydrogenated NH groups in the correlation loading plot in Figure 3a, which shows that the increase of aggregated structures with high salt concentrations is related to a decrease of α-helical structures in the studied myofibrillar proteins. This finding is in agreement with the literature,[16,31] where a rise in NaCl concentration in brine salting of pork meat was found to induce an increase in nonhydrogenated C═O groups and aggregated β-structures at the expense of native α-helical structures.[16,33,43] On the other hand, the amide I band occurring at around 1618 cm^{-1} is tentatively assigned to aggregated β-structures.[17,33,43] This finding is not in accordance with our results, where this band is often correlated to the lowest salt concentration (most of these results not shown here) and to bands that are assigned to hydrogenated NH groups. In our data the band at 1618 cm^{-1} also exhibits a *negative* correlation tendency toward aggregated β-structures (that are mostly detectable through the band at 1631 cm^{-1}). However, in our results this band does not show any clear pattern in correlation tendencies and therefore remains not assigned.

Along with this, the water region (3500−3000 cm^{-1}) presented in Figure 1b consists mostly of N−H stretching vibrations and O−H stretching bands.[19,22] Analysis of the score plots of the PCA of the water region in Figure 2c,d shows that the main variation pattern in the water region is caused by different salt types. Within each salt type cluster there are visible concentration differences, but they are obviously less pronounced than the differences due to salt type, meaning that the differences between types of salts applied cause larger alterations in protein hydration than differences in applied salt concentrations. Whereas the first component to some extent separates the NaCl samples from the KCl samples, the second component shows a clear separation of $MgSO_4$ from the NaCl- and the KCl-treated samples. In the corresponding correlation loading plot in Figure 3b it can be seen that the region 3500−3450 cm^{-1} is *positively* correlated to $MgSO_4$ salt type in high concentrations. In this region is located the intermolecular ν_{O-H} stretching band. It is most pronounced in liquid water spectra with a maximum around 3430−3420 cm^{-1} and is also present in dry hydrated biomolecules with a shift toward lower wavenumber due to smaller amount of H-bonds.[19] This is in correspondence with the WBC results (Figure 6) that show highest WBC for samples treated with 9% $MgSO_4$ (4.5% of expressed juice compared to 5.1% of NaCl and 8.4% of KCl). As can be seen in Figure 3b, the ν_{O-H} stretching band exhibits a shift stretching from 3411 cm^{-1} close to the design variable 9% NaCl to the design variable 9% $MgSO_4$ while passing close by the design variable 9% concentration. This shows that hydration is increased for higher salt concentrations and that there are some interaction effects between the salt type factors of NaCl and $MgSO_4$ and the concentration factor of 9%, corresponding also to the similarities found in the values of WBC for these two salt types.

To address the protein structural information directly, the information about water binding in the amide I region was related to the water region by PLSR. The corresponding correlation loading plot is shown in Figure 4a. In this figure the same tendencies as in Figure 3a,b can be observed, with a difference that in Figure 4a the relationship between the water binding and the protein region is much clearer. In addition to this, increased salt concentration causes an increment of intensity in the intermolecular ν_{O-H} stretching occurring around 3430−3420 cm^{-1}. This is the case for $MgSO_4$ and NaCl brines, but not for KCl brines. This is also apparent in WBC measurements, where KCl-treated samples exhibit the lowest WBC, whereas NaCl and $MgSO_4$ brines cause effects similar to the WBC of the meat samples. Moreover, there is a clear interaction effect visible between the $MgSO_4$ and NaCl salt types and the 9% salt concentration, whereas the interaction variable 9% KCl is not related to high hydration levels. It can also be seen that the increase of hydration is closely related to the aggregated β-structures. This again can be interpreted in the way that, with increasing hydration, proteins unfold and increase the WBC by exposing larger parts of the protein molecules to water.[44,45] The exposure of the hydrophobic part leads then finally to a destabilization and partial denaturation of the myofibrillar proteins at the highest salt concentrations (in addition to thermal effects and effects of pH),[46] which is expressed by the *positive* correlation of the band at ∼1631 cm^{-1} with the interaction variables 9% $MgSO_4$ and 9% NaCl and the concentration variable 9% in Figures 3b and Figure 4a.

In Figures 3b and 4 it can also be seen that there is a remarkably strong correlation between the hydration bands (around 3430−3420 cm^{-1}), the water or aggregated β-structure band at 1638 cm^{-1}, and the interaction factor 9% $MgSO_4$ and the salt type $MgSO_4$. At the same time there is also a clear correlation between this hydration band and the band of aggregated β-structures. A correspondingly strong correlation between aggregated β-structures around 1631 cm^{-1} and the interaction variable 9% $MgSO_4$ can be seen. It seems that $MgSO_4$ has a stronger effect on hydration and denaturation of the proteins than NaCl. Because the effect of salts alone in the applied concentrations is not sufficient for complete unfolding and denaturation of

proteins, it is likely that the investigated proteins are partially unfolded and therefore their hydration is notably altered in a direction of increased hydration. We may also hypothesize that $MgSO_4$ causes higher partial denaturation and increased subsequent hydration at lower concentrations than NaCl. To investigate this more closely, we considered PCA plots of the samples treated with 1.5, 6, and 9% brines separately. It turned out that $MgSO_4$ had strong hydration and denaturation effects already at 6% concentration, whereas this was not as pronounced for NaCl (see Figure 5). At 9% concentration both salt types gave similar denaturation effects (results not shown), whereas KCl showed less denaturation even at the 9% concentration. This finding is in accordance with the Hofmeister series, which attributes SO_4^{2-} with a higher salting-out effect than Cl^-.[47−49] An increased hydration of the proteins in meat tissue is related to their partial unfolding and to protein destabilization as a final outcome.[44,50] This unfolding of the protein can lead to an increase of hydration at moderate salt concentrations, because large parts of the proteins are exposed to the solvent environment and are able to bind water molecules. According to our findings, $MgSO_4$ salt brines increase the hydration properties of myofibrillar proteins more efficiently with increasing salt concentration than NaCl and KCl. Therefore, the myofibrillar proteins also denature more rapidly with increasing salt concentration in the samples with $MgSO_4$ compared with samples treated with NaCl or KCl. This finding is also supported by measurements of WBC of samples treated with these salts. This finding may be utilized in the meat industry by replacing NaCl partially with lower amounts of $MgSO_4$.

As shown, FTIR microscopy in combination with chemometrical tools can be used to monitor changes in muscle proteins caused by different salt types and concentrations. In addition to the most commonly used amide I region, the amide II and water regions (3500−3000 cm^{-1}) are also shown to be sensitive to these minute changes in secondary structure and hydration properties. The water region in particular expressed a potential for assessing the differences in hydration properties in proteins and to supplement the information on secondary structure changes obtained by inspecting the amide I region. Moreover, the results obtained by WBC measurements show a high correspondence to the results obtained by FTIR microscopy. This again shows that the changes in the secondary structure of the myofibrillar proteins can be connected to macroscopic properties of meat, such as WBC. Additionally, although KCl is widely used as a substitute for NaCl,[6,9,10] it showed distinctive differences when it comes to secondary structure of meat proteins and their hydration properties. On the contrary, $MgSO_4$ exhibited certain similarities to NaCl, which might imply that the mechanism of interaction between this salt ion and protein molecules is intrinsically complex.

AUTHOR INFORMATION

Corresponding Author

*Postal address: Nofima AS, Osloveien 1, 1430 Ås, Norway. Phone: +47 64 97 01 00. Fax: +47 64 97 03 33. E-mail: nebojsa.perisic@nofima.no.

Funding Sources

This work was supported by Grant 185063/I10 financed by the Research Council of Norway. Financial support from the Agricultural Food Research Foundation of Norway is also gratefully acknowledged.

ACKNOWLEDGMENT

We thank Karin Solgaard, Bjørg Narum, and Karen Wahlstrøm Sanden for technical assistance and Sahar Hassani for programming support in Matlab.

REFERENCES

(1) Cappuccio, F. P.; Markandu, N. D.; Carney, C.; Sagnella, G. A.; MacGregor, G. A. Double-blind randomised trial of modest salt restriction in older people. *Lancet* **1997**, *350* (9081), 850–854.

(2) Cappuccio, F. P.; Kalaitzidis, R.; Duneclift, S.; Eastwood, J. B. Unravelling the links between calcium excretion, salt intake, hypertension, kidney stones and bone metabolism. *J. Nephrol.* **2000**, *13*, 169–177.

(3) Chrysant, G. S. High salt intake and cardiovascular disease: is there a connection? *Nutrition* **2000**, *16* (7−8), 662–664.

(4) Ruusunen, M.; Puolanne, E. Reducing sodium intake from meat products. *Meat Sci.* **2005**, *70* (3), 531–541.

(5) Desmond, E. Reducing salt: a challenge for the meat industry. *Meat Sci.* **2006**, *74* (1), 188–196.

(6) Kilcast, D.; Angus, F. *Reducing Salt in Foods − Practical Strategies*; Woodhead Publishing: Cambridge, U.K., 2007.

(7) Offer, G.; Knight, P.; Jeacocke, R.; Almond, R.; Cousins, T.; Elsey, J.; Parsons, N.; Sharp, A.; Starr, R.; Purslow, P. The structural basis of the water-holding, appearance and toughness of meat and meat products. *Food Nicrostruct.* **1989**, *8* (1), 151–170.

(8) He, F. J.; MacGregor, G. A. A comprehensive review on salt and health and current experience of worldwide salt reduction programmes. *J. Hum. Hypertens.* **2008**, *23* (6), 363–384.

(9) Guàrdia, M. D.; Guerrero, L.; Gelabert, J.; Gou, P.; Arnau, J. Sensory characterisation and consumer acceptability of small calibre fermented sausages with 50% substitution of NaCl by mixtures of KCl and potassium lactate. *Meat Sci.* **2008**, *80* (4), 1225–1230.

(10) Gimeno, O.; Astiasarán, I.; Bello, J. Influence of partial replacement of NaCl with KCl and $CaCl_2$ on microbiological evolution of dry fermented sausages. *Food Microbiol.* **2001**, *18* (3), 329–334.

(11) Samapundo, S.; Ampofo-Asiama, J.; Anthierens, T.; Xhaferi, R.; Van Bree, I.; Szczepaniak, S.; Goemaere, O.; Steen, L.; Dhooge, M.; Paelinck, H.; Dewettinck, K.; Devlieghere, F. Influence of NaCl reduction and replacement on the growth of *Lactobacillus sakei* in broth, cooked ham and white sauce. *Int. J. Food Microbiol.* **2010**, *143* (1−2), 9–16.

(12) Gou, P.; Guerrero, L.; Gelabert, J.; Arnau, J. Potassium chloride, potassium lactate and glycine as sodium chloride substitutes in fermented sausages and in dry-cured pork loin. *Meat Sci.* **1996**, *42* (1), 37–48.

(13) Guàrdia, M. D.; Guerrero, L.; Gelabert, J.; Gou, P.; Arnau, J. Consumer attitude towards sodium reduction in meat products and acceptability of fermented sausages with reduced sodium content. *Meat Sci.* **2006**, *73* (3), 484–490.

(14) Crehan, C. M.; Troy, D. J.; Buckley, D. J. Effects of salt level and high hydrostatic pressure processing on frankfurters formulated with 1.5 and 2.5% salt. *Meat Sci.* **2000**, *55* (1), 123–130.

(15) Selgas, M. D.; Salazar, P.; García, M. L. Usefulness of calcium lactate, citrate and gluconate for calcium enrichment of dry fermented sausages. *Meat Sci.* **2009**, *82* (4), 478–480.

(16) Böcker, U.; Ofstad, R.; Bertram, H. C.; Egelandsdal, B. R.; Kohler, A. Salt-induced changes in pork myofibrillar tissue investigated by FT-IR microspectroscopy and light microscopy. *J. Agric. Food Chem.* **2006**, *54* (18), 6733–6740.

(17) Wu, Z.; Bertram, H. C.; Boecker, U.; Ofstad, R.; Kohler, A. Myowater dynamics and protein secondary structural changes as affected by heating rate in three pork qualities: a combined FT-IR microspectroscopic and ^1H NMR relaxometry study. *J. Agric. Food Chem.* **2007**, *55* (10), 3990–3997.

(18) Bertram, H. C.; Kohler, A.; Bocker, U.; Ofstad, R.; Andersen, H. J. Heat-induced changes in myofibrillar protein structures and myowater of two pork qualities. A combined FT-IR spectroscopy and low-field NMR relaxometry study. *J. Agric. Food Chem.* **2006**, *54* (5), 1740–1746.

(19) Maréchal, Y. Interaction configurations of H_2O molecules in a protein (Stratum Corneum) by infrared spectrometry. *J. Mol. Struct.* **1997**, *416* (1−3), 133–143.

(20) Jackson, M.; Mantsch, H. H. The use and misuse of FTIR spectroscopy in the determination of protein structure. *Crit. Rev. Biochem. Mol. Biol.* **1995**, *30* (2), 95–120.

(21) Grdadolnik, J. A FTIR investigation of protein conformation. *Bull. Chem. Technol. Maced* **2002**, *21*, 23–34.

(22) Barth, A. Infrared spectroscopy of proteins. *Biochim. Biophys. Acta (BBA): Bioenerg.* **2007**, *1767* (9), 1073–1101.

(23) Wierbicki, E.; Deatherage, F. E. Water content of meats, determination of water-holding capacity of fresh meats. *J. Agric. Food Chem.* **1958**, *6* (5), 387–392.

(24) Savitzky, A.; Golay, M. Smoothing and differentiation of data by simplified least squares procedures. *Anal. Chem.* **1964**, *36* (8), 1627–1639.

(25) Kohler, A.; Kirschner, C.; Oust, A.; Martens, H. Extended multiplicative signal correction as a tool for separation and characterization of physical and chemical information in Fourier transform infrared microscopy images of cryo-sections of beef loin. *Appl. Spectrosc.* **2005**, *59* (6), 707–716.

(26) Martens, H.; Nielsen, J. P.; Engelsen, S. B. Light scattering and light absorbance separated by extended multiplicative signal correction. Application to near-infrared transmission analysis of powder mixtures. *Anal. Chem.* **2003**, *75* (3), 394–404.

(27) Martens, H.; Næs, T. *Multivariate Calibration*; Wiley: Chichester, U.K., 1989.

(28) Martens, H.; Martens, M. Multivariate analysis of quality. An introduction. *Meas. Sci. Technol.* **2001**, *12* (10), 1746.

(29) Golub, G. H.; Heath, M.; Wahba, G. Generalized cross-validation as a method for choosing a good ridge parameter. *Technometrics* **1979**, *21* (2), 215–223.

(30) Efron, B. Estimating the error rate of a prediction rule: improvement on cross-validation. *J. Am. Stat. Assoc.* **1983**, *78* (382), 316–331.

(31) Bocker, U.; Ofstad, R.; Wu, Z. Y.; Bertram, H. C.; Sockalingum, G. D.; Manfait, M.; Egelandsdal, B.; Kohler, A. Revealing covariance structures in Fourier transform infrared and Raman microspectroscopy spectra: a study on pork muscle fiber tissue subjected to different processing parameters. *Appl. Spectrosc.* **2007**, *61* (10), 1032–1039.

(32) Barth, A.; Zscherp, C. What vibrations tell about proteins. *Q. Rev. Biophys.* **2002**, *35* (04), 369–430.

(33) Böcker, U.; Ofstad, R.; Wu, Z.; Bertram, H. C.; Sockalingum, G. D.; Manfait, M.; Egelandsdal, B.; Kohler, A. Revealing covariance structures in Fourier transform infrared and raman microspectroscopy spectra: a study on pork muscle fiber tissue subjected to different processing parameters. *Appl. Spectrosc.* **2007**, *61* (10), 1032–1039.

(34) Surewicz, W. K.; Mantsch, H. H.; Chapman, D. Determination of protein secondary structure by Fourier transform infrared spectroscopy: a critical assessment. *Biochemistry* **1993**, *32* (2), 389–394.

(35) Manas, E.; Getahun, Z.; Wright, W.; DeGrado, W.; Vanderkooi, J. Infrared spectra of amide groups in α-helical proteins: evidence for hydrogen bonding between helices and water. *J. Am. Chem. Soc.* **2000**, *122* (41), 9883–9890.

(36) Boubellouta, T.; Galtier, V.; Dufour, É. Structural changes of milk components during acid-induced coagulation kinetics as studied by synchronous fluorescence and mid-infrared spectroscopy. *Appl. Spectrosc.* **2010**, *65* (3), 284–292.

(37) Nevskaya, N. A.; Chirgadze, Y. N. Infrared spectra and resonance interactions of amide-I and II vibrations of α-helix. *Biopolymers* **1976**, *15* (4), 637–648.

(38) Rothschild, K. J.; Clark, N. A. Polarized infrared spectroscopy of oriented purple membrane. *Biophys. J.* **1979**, *25* (3), 473–487.

(39) Liltorp, K.; Maréchal, Y. Hydration of lysozyme as observed by infrared spectrometry. *Biopolymers* **2005**, *79* (4), 185–196.

(40) Barth, A. The infrared absorption of amino acid side chains. *Prog. Biophys. Mol. Biol.* **2000**, *74* (3−5), 141–173.

(41) Fabian, H.; Schultz, C. P. *Fourier Transform Infrared Spectroscopy in Peptide and Protein Analysis*; Wiley: Chichester, U.K., 2006.

(42) Abe, Y.; Krimm, S. Normal vibrations of crystalline polyglycine I. *Biopolymers* **1972**, *11* (9), 1817–1839.

(43) Bertram, H. C.; Kohler, A.; Boecker, U.; Ofstad, R.; Andersen, H. J. Heat-induced changes in myofibrillar protein structures and myowater of two pork qualities. A combined FT-IR spectroscopy and low-field NMR relaxometry study. *J. Agric. Food Chem.* **2006**, *54* (5), 1740–1746.

(44) Stigter, D.; Aalonso, D. O. V.; Dill, K. A. *Protein Stability: Electrostatics and Compact Denatured States*; National Academy of Sciences: Washington, DC, 1991; Vol. 88, p 5.

(45) Dill, K. A. Dominant forces in protein folding. *Biochemistry* **1990**, *29* (31), 7133–7155.

(46) Ishii, Y. The local and global unfolding of coiled-coil tropomyosin. *Eur. J. Biochem.* **1994**, *221* (2), 705–712.

(47) Baldwin, R. L. How Hofmeister ion interactions affect protein stability. *Biophys. J.* **1996**, *71* (4), 2056–2063.

(48) Giner, I.; Pera, G.; Lafuente, C.; López, M. C.; Cea, P. Influence of the Hofmeister series of anions on the molecular organization of positively ionized monolayers of a viologen derivative. *J. Colloid Interface Sci.* **2007**, *315* (2), 588–596.

(49) Lawal, O. S. Kosmotropes and chaotropes as they affect functionality of a protein isolate. *Food Chem.* **2006**, *95* (1), 101–107.

(50) Hofmeister, F. Zur lehre von der wirkung der salze. *Naunyn-Schmiedeberg's Arch. Pharmacol.* **1888**, *25* (1), 1–30.

(51) Wu, Z.; Bertram, H. C.; Kohler, A.; Boecker, U.; Ofstad, R.; Andersen, H. J. Influence of aging and salting on protein secondary structures and water distribution in uncooked and cooked pork. A combined FT-IR microspectroscopy and ^{1}H NMR relaxometry study. *J. Agric. Food Chem.* **2006**, *54* (22), 8589–8597.

(52) Pevsner, A.; Diem, M. Infrared spectroscopic studies of major cellular components. Part I: The effect of hydration on the spectra of proteins. *Appl. Spectrosc.* **2001**, *55* (6), 788–793.

(53) Silvestrelli, P. L.; Bernasconi, M.; Parrinello, M. Ab initio infrared spectrum of liquid water. *Chem. Phys. Lett.* **1997**, *277* (5−6), 478–482.

(54) Taylor, J. R. *An Introduction to Error Analysis: The Study of Uncertainties in Physical Measurements*; University Science Books: Herndon, VA, 1997.